

The Floquet central spin model: A platform to realize eternal time crystals, entanglement steering, and multiparameter metrology

Hillol Biswas¹ and Sayan Choudhury^{1,*}

¹Harish-Chandra Research Institute, a CI of Homi Bhabha National Institute, Chhatnag Road, Jhansi, Allahabad 211019
(Dated: January 31, 2025)

We propose and characterize protocols to realize eternal discrete time crystals (DTCs) in the periodically driven central spin model. These eternal DTCs exhibit perfect periodic revivals of the initial state at a time mnT (where $n > 1$ and $\{m, n\} \in \mathbb{Z}$), when the Ising interaction strength, λ between the central spin and the satellite spins is tuned to certain values. The combination of perfect initial-state revival and time-translation-symmetry breaking leads to infinitely long-lived oscillations of the stroboscopic magnetization and the entanglement entropy in these DTCs even for a finite number of satellite spins. We analytically determine the conditions for the existence of these eternal DTCs and prove that the system exhibits eternal period-doubling oscillations ($n = 2$) when $\lambda = 2\pi$ for an arbitrary number of satellite spins. Furthermore, we propose a protocol to realize eternal higher-order(HO)-DTCs ($n > 2$) by tuning λ to π . Intriguingly, this protocol naturally steers the system through an entangled trajectory, thereby leading to the generation of maximally entangled Bell-cat states during the dynamical evolution of the HO-DTC. Finally, we demonstrate that these HO-DTCs can serve as a resource for Heisenberg-limited multiparameter sensing.

Introduction: Periodically driven (Floquet) quantum systems host non-equilibrium phases of matter with no equilibrium analog [1–6]. One of the most striking examples of a Floquet phase of matter is a discrete time crystal (DTC) [7–11]. DTCs are characterized by discrete time-translation-symmetry-breaking (TTSB) and a consequent sub-harmonic response of physical observables [12–14]. Apart from its fundamental importance as a non-equilibrium phase of matter, DTCs are also expected to be useful for applications in quantum technologies [15, 16]. DTCs have now been experimentally realized in various platforms including trapped ion chains [17, 18], Carbon-13 nuclear spins in diamond [19–21], Rydberg atom arrays [22, 23], superconducting quantum processors [24–26].

Interactions are crucial for stabilizing TTSB and realizing a robust DTC [27, 28]. Unfortunately, interacting Floquet systems generically heat up to a featureless temperature state [29–32], thereby posing a major challenge to realizing a DTC [33]. Consequently, the initial realization of DTCs relied crucially on many-body localization to evade Floquet heating [17]. However, in later years, several studies have demonstrated the possibility of realizing a DTC without disorder [34–45]. One of the most celebrated examples of such a disorder-free DTC is in the Floquet central spin model, where long-lived period-doubling oscillations of the magnetization have been theoretically predicted [46–48] and experimentally observed [36, 49].

In this Letter, we unveil several new features of this system that have not been observed before. Firstly, we propose a route to realize eternal period-doubling oscillations in this system for an arbitrary number of satellite spins. Secondly, we present a protocol to realize an eternal ‘higher-order’ (HO)-DTC [39], where physical observables such as the magnetization and the entangle-

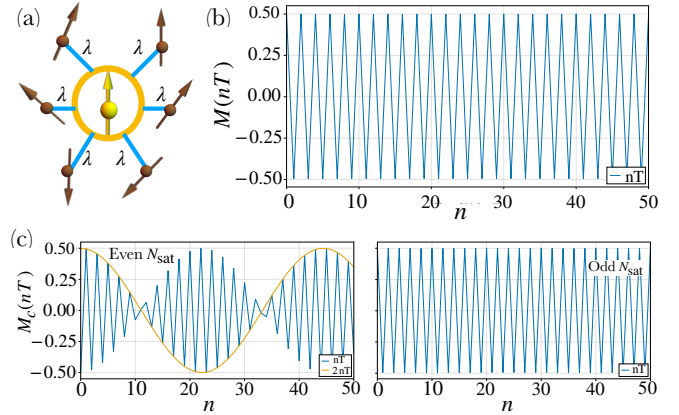


FIG. 1. **Model and DTC dynamics:** (a) A schematic illustration of the central spin model where one central spin-1/2 particle is coupled to N_{sat} – non-interacting satellite spin-1/2 particles. Each satellite spin interacts with the central spin with a strength λ . (b) The satellite spin magnetization, $M(nT)$ exhibits eternal period-doubling oscillations when $\lambda = 2\pi$ due to a many-body echo mechanism (Eq. 2). (c) The many-body echo mechanism leads to eternal period-doubling oscillations of the central spin magnetization, $M_c(nT)$, only when N_{sat} is odd.

ment entropy oscillate with a period longer than $2T$; the dynamical evolution of such DTCs leads to the creation of maximally entangled Bell-cat states [50]. Crucially, both protocols mentioned above utilize a many-body echo mechanism that leads to a perfect initial state revival at a time mnT , where $n > 1$ and $\{m, n\} \in \mathbb{Z}$. Finally, we perform a detailed analysis of the sensing capabilities of these eternal HO-DTCs and find that they can be employed for Heisenberg-limited sensing of the interaction strength and external magnetic fields.

Period-doubling DTC: We explore the dynamics of a periodically driven system composed of a central spin ($S^{(c)}$) interacting with N_{sat} satellite (or ancilla) spins (S^i) with an Ising interaction λ :

$$H(t) = \begin{cases} H_d = \frac{2}{T}(g_s \sum_{i=1}^{N_{\text{sat}}} S_i^z + g_c S_c^z) & \text{for } t \in [0, T/2) \\ H_0 = -2\lambda \sum_{i=1}^{N_{\text{sat}}} S_i^x S_c^x & \text{for } t \in [T/2, T). \end{cases} \quad (1)$$

Here $S^\gamma = \frac{1}{2}\sigma^\gamma$, where σ^γ are the Pauli matrices, and g_c and g_s are the strengths of the magnetic fields acting on the central and satellite spins, respectively; we set $T = 1$ for our calculations. A schematic illustration of the model is shown in Fig. 1(a). This model can be realized in quantum dots [51], ultracold atomic gases [52, 53], nitrogen-vacancy centers in diamond [54, 55], and solid-state nuclear magnetic resonance [56].

We now proceed to discuss a mechanism to realize eternal period-doubling oscillations of the satellite spin magnetization for any value of g_s and g_c by tuning λ to 2π . These perfect period-doubling oscillations occur for all values of N_{sat} , as illustrated in Fig. 1(b). We note however that dynamics of the central spin depend crucially on the number of satellite spins, N_{sat} and perfect period-doubling oscillations occur only when N_{sat} is odd. For even N_{sat} the stroboscopic central spin magnetization changes sinusoidally. To elucidate the origin of these observations, we note that the Floquet unitary can be written as $U_F = U(T, 0) = U_0 U_d$, where $U_0 = \exp[-iH_0 T/2]$ and $U_d = \exp[-iH_d T/2]$. A many-body echo protocol is implemented when $\lambda = 2\pi$, since S_j^z anti-commutes with U_0 , leading to the following the time-evolution operator after 2 periods:

$$U(2T, 0) = U_F^2 = U_0 (\exp[-ig_c S_c^z] \otimes \mathbb{I}_{\text{sat}}) U_0 \exp[-ig_c S_c^z], \quad (2)$$

where \mathbb{I} represents the Identity matrix. Furthermore, U_c commutes (anti-commutes) with U_d when the number of satellite spins are even (odd). Thus, for an odd number of satellite spins, $U(2T, 0) = \mathbb{I}$, thereby leading to a perfect revival of the initial state of both the central and satellite spins. However, when the number of satellite spins is even, $U(2T, 0) = \exp[-i2g_c S_c^z] \otimes \mathbb{I}_{\text{sat}}$, thereby leading to a perfect revival (sinusoidal oscillations) of the magnetization of the satellite (central) spins. Crucially, this analysis holds for every initial state and these results remain unchanged if the magnetic field g_s acting on each satellite spin is different, thereby highlighting the robustness of this non-ergodic behavior.

Our analysis so far has established the existence of a perfect revival of the initial state at $\lambda = 2\pi$ for any value of g_s and g_c . Next, we analyze the robustness of this initial state memory retention for other parameter values, by computing the time-averaged magnetization at times $2nT$: $\langle \bar{M} \rangle = \frac{1}{N} \sum_{n=1}^N M(2nT)$, (where $M = \sum_{i=1}^{N_{\text{sat}}} S_i^x$) for the fully x-polarized initial state, $|\psi(t=0)\rangle = \left(\prod_{i=1}^{N_{\text{sat}}} |+\rangle_i\right) \otimes |+\rangle_c$, where $|\pm\rangle$ are

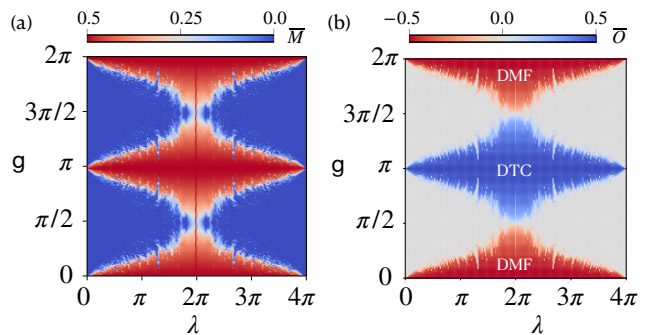


FIG. 2. Dynamical many-body freezing and period-doubling DTCs: (a) Density plot of the time-averaged magnetization at $t = 2nT$, $\bar{M} = \frac{1}{500} \sum_{n=1}^{500} M(2nT)$, when $g_s = g_c = g$. The system exhibits a perfect revival at $t = 2nT$ for $g = j\pi \forall \lambda$ and $\lambda = 2j\pi \forall g$, where $j \in \mathbb{Z}$. Apart from these points, the system exhibits non-ergodic dynamics for a large parameter regime. (b) Density plot of the time-averaged order parameter, \bar{O} (eq. 3): $\bar{O} = (1/N) \sum_{i=1}^N O(nT)$ shows that there is a wide parameter regime where the system exhibits DTC ($\bar{O} \sim 0.5$) and DMF ($\bar{O} \sim -0.5$) behaviors. The results presented here are for $N_{\text{sat}} = 19$

the eigenstates of σ_x with eigenvalues of ± 1 . As shown in fig. 2(a), there is a large parameter regime where the system exhibits initial state memory retention, as indicated by a large value of $\langle \bar{M} \rangle$.

We note that a perfect initial state revival at times $2nT$ can be associated with two kinds of non-ergodic behavior: (i) dynamical many-body freezing (DMF), where the system approximately returns to its initial state at times nT [57–61], and (ii) a DTC characterized by TTSB and a sub-harmonic response of physical observables [7, 9, 10]. An eternal DTC exhibiting perfect period-doubling oscillations would emerge when $g = 2n\pi$ ($g = (2n+1)\pi$, with $n \in \mathbb{Z}$ for any value of λ). To characterize the non-ergodic dynamics in other regions of parameter space, we define a new order parameter:

$$O(nT) = O_{\text{DTC}}(nT) - O_{\text{DMF}}(nT), \quad \text{where} \\ O_{\text{DTC}}(nT) = (-1)^n M(nT) \quad \text{and} \quad O_{\text{DMF}}(nT) = M(nT). \quad (3)$$

The order parameters, O_{DTC} and O_{DMF} have been conventionally employed to characterize the DMF and DTC phases. We characterize DTC and DMF behavior by computing the time-averaged value of O : $\bar{O} = (1/N) \sum_{i=1}^N O(nT)$; $\bar{O} \sim 0.5$ characterizes a DTC and $\bar{O} \sim -0.5$ characterizes DMF. An analytical explanation for the transition between DTC and DMF behaviors for $\lambda = 2\pi$ is presented in ref [62]. Figure 2(b) shows that is a wide parameter regime where the system exhibits DMF and DTC behaviors, thereby demonstrating the rich non-ergodic behavior in the system that arises from our proposed many-body echo protocol.

Higher-order DTC and entanglement steering: Having established the existence of a robust period-doubling DTC, we now proceed to examine whether this model can host HO-DTC phases. A HO-DTC emerges when a \mathbb{Z}_N -symmetric system exhibits persistent order parameter oscillations with a period pT , with $p > N$ [39, 63]. In our case, the underlying Hamiltonian (eq. 1) has a \mathbb{Z}_2 symmetry; thus, a HO-DTC would be characterized by oscillations with a period larger $2T$. Interestingly, we find that the system can exhibit persistent oscillations of physical observables with a period of $12T$ ($24T$) for odd (even) values of N_{sat} , when $\lambda \sim (2n + 1)\pi$ and $g_s = g_c = g \sim (2m + 1)\pi/2$, where $\{n, m\} \in \mathbb{Z}$; these oscillations never decay when $\lambda = (2n + 1)\pi$ and $g = (2m + 1)\pi/2$. To illustrate this, we have examined the time-evolution of the fully x-polarized initial state, $|\psi(t=0)\rangle = \left(\prod_{i=1}^{N_{\text{sat}}} |+\mathbf{x}\rangle_i\right) |+\mathbf{x}\rangle_c$. As shown in fig. 3(a), the system exhibits eternal magnetization oscillations, when $\lambda = \pi$ and $g = \pi/2$. We note that the central and satellite spin magnetizations oscillate with a period of $8T$ ($12T$) and $24T$ ($12T$) respectively, when N_{sat} is odd (even).

We now proceed to examine the states that are generated during the time evolution of the DTC. Intriguingly, we find that our protocol naturally leads to the generation of maximally entangled Bell-cat states [50, 64] at times $3qT$, where $q \in \mathbb{Z}$. We first analyze the time-evolution of this system when N_{sat} is even. In this case at $t = 3T$, the system evolves to the entangled Bell-cat state $|\phi^{(\text{BC})}\rangle$:

$$|\phi_{\pm}^{(\text{BC})}\rangle = \frac{1}{\sqrt{2}} \left(\prod_{j=1}^{N_{\text{sat}}} |+\mathbf{x}\rangle_j \right) |\pm\mathbf{x}\rangle_c + \alpha \left(\prod_{j=1}^{N_{\text{sat}}} |-\mathbf{x}\rangle_j \right) |\mp\mathbf{x}\rangle_c, \quad (4)$$

where $|\phi_{+}^{(\text{BC})}\rangle$ ($|\phi_{-}^{(\text{BC})}\rangle$) with $\alpha = +i$ corresponds to $N_{\text{sat}} = 4j$ ($4j + 2$) for $j \in \mathbb{Z}$. Naturally, in both of these cases, $|\psi(t = 6T)\rangle = \left(\prod_{j=1}^{N_{\text{sat}}} |-\mathbf{x}\rangle_j\right) |-\mathbf{x}\rangle_c$, and the system returns to its initial state, $\left(\prod_{j=1}^{N_{\text{sat}}} |+\mathbf{x}\rangle_j\right) |+\mathbf{x}\rangle_c$ at $t = 12T$. This leads to eternal oscillations of the magnetization with a period of $12T$.

The time-evolution of the system when N_{sat} is odd is more intricate, and a detailed discussion is provided in ref. [62]; here we discuss some important aspects of this dynamics. We start by noting that even though the states generated during the time-evolution of the system is different when $N_{\text{sat}} = 4j + 1$ or $N_{\text{sat}} = 4j + 3$ ($j \in \mathbb{Z}$), in both of these situations at $t = 4T$, the system is in the state:

$$|\psi(t = 4T)\rangle = \frac{1}{\sqrt{2}} \left[\left(\prod_{j=1}^{N_{\text{sat}}} |+\mathbf{z}\rangle_j \right) - \left(\prod_{j=1}^{N_{\text{sat}}} |-\mathbf{z}\rangle_j \right) \right] |-\mathbf{x}\rangle_c \quad (5)$$

where $|\pm\mathbf{z}\rangle$ represent the eigenstates of σ_z , corresponding to the eigenvalues of ± 1 . This leads to eternal oscillations

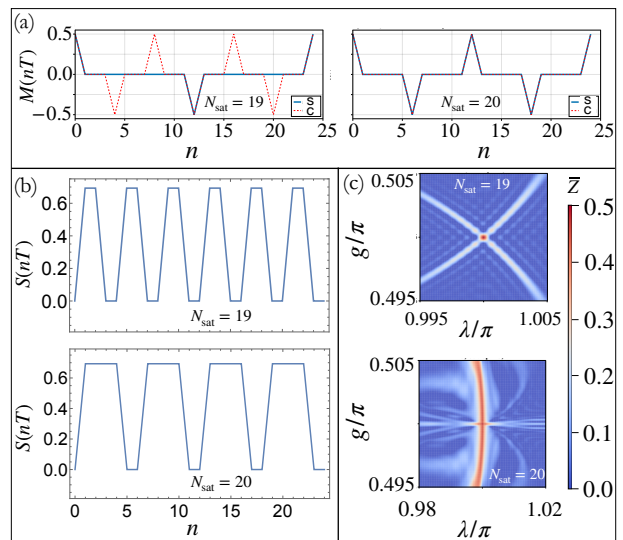


FIG. 3. Dynamics of Higher-order DTC: (a) The time-evolution of the satellite spin magnetization (solid blue) central spin magnetization (dashed red line) when $\lambda = \pi$ and $g = \pi/2$. When N_{sat} is odd, the satellite spin (central spin) magnetization oscillates eternally with a period of $24T$ ($8T$). For even N_{sat} , both the satellite and central spin magnetization oscillate with a period of $12T$. (b) The entanglement between the central and satellite spins oscillate with a period of $4T$ ($6T$) when N_{sat} is odd (even). These entanglement oscillations lead to the generation of Bell-cat states. (c) Density plot of the time-averaged order parameter, \bar{Z} (Eq. 6 for $N_{\text{sat}} = 19$ and 20). The stability of the DTCs are enhanced when N_{sat} is even.

of the central spin magnetization with a period of $8T$. Interestingly, $|\psi(t = 4t)\rangle$ can be useful as a resource for magnetic field sensing, since the satellite spins are in a ‘spin-cat’ state [65, 66]. Moreover, after 6 periods the system evolves to the Bell-cat state $|\phi_{+}^{(\text{BC})}\rangle$ (defined in eq. 4) with $\alpha = -i$. This in turn leads to the state $\left(\prod_{j=1}^{N_{\text{sat}}} |-\mathbf{x}\rangle_j\right) |-\mathbf{x}\rangle_c$ at $t = 12T$, which leads to oscillations of satellite spin magnetization with a period of $24T$.

Next, we examine the dynamics of the entanglement between the central and satellite spins by $S = -\rho_c \ln(\rho_c)$, where ρ_c is the reduced density matrix of the central spin. Our analysis shown in fig. 3(b) shows that our protocol steers the system through an entangled trajectory, where the entanglement entropy oscillates with a period of $4T$ and $6T$ for odd and even values of N_{sat} respectively. Finally, analogous to our analysis of the period-doubling DTC, we have studied the robustness of the HO-DTC by computing the time-averaged order parameter, \bar{Z} :

$$\bar{Z} = \frac{1}{N} \sum_{n=1}^{\beta} Z_n, \quad \text{where } Z_n = (-1)^n M(\alpha n T). \quad (6)$$

We have set $\beta = 200(100)$ and $\alpha = 6(12)/\pi$ for even (odd) N in our calculations; the results are shown in fig. 3(c).

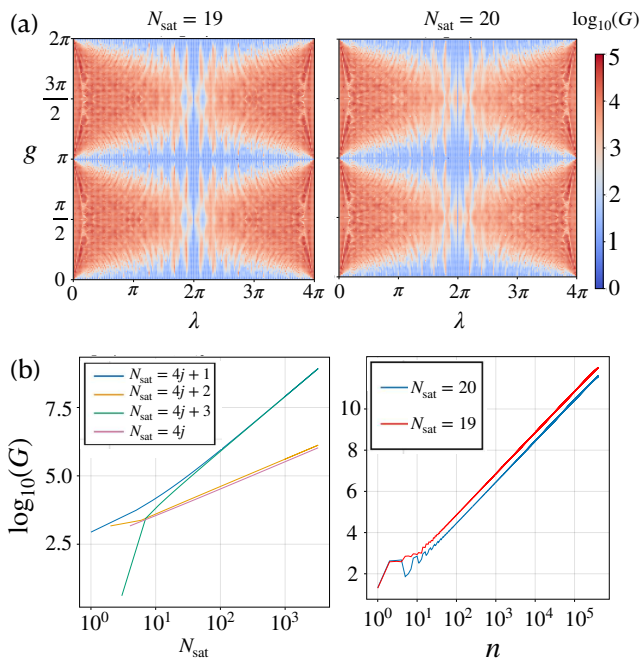


FIG. 4. **Quantum metrology with HO-DTCs:** (a) The density plot of G (Eq. 7), when $N_{\text{sat}} = 19$ and 20 . The HO-DTC phase is associated with a high value of G , thereby making it a powerful resource for multi-parameter metrology (b) Scaling of G with the number of satellite spins, N_{sat} (left panel) when $t = 100T$ and the number of drive periods, n (right panel) when $\lambda = \pi$ and $g = \pi/2$. For odd and even values of N_{sat} , $G \propto n^2 N_{\text{sat}}^2$ (Heisenberg limit) and $G \propto n^2 N_{\text{sat}}$ respectively. These results demonstrate that HO-DTCs can exhibit quantum-enhanced sensitivity.

We note that although the HO-DTCs are more fragile than their period-doubling counterparts, the robustness of these DTCs are considerably enhanced, when N_{sat} is even. Our results provide a pathway to realize HO-DTCs by entanglement steering.

Multi-parameter quantum metrology: We have demonstrated that the Floquet central-spin model can exhibit eternally long-lived oscillations of physical observables, when $\lambda = n\pi$, where $n \in \mathbb{Z}$. We now demonstrate that eternal HO-DTCs can be employed for quantum-enhanced sensing of the interaction strength, λ and the magnetic field, g . In order to characterize this sensitivity, we note that the uncertainty in measuring a parameter λ and g can be obtained from the 2×2 quantum Fisher information matrix, \mathcal{F} , whose elements are given by: $\mathcal{F}_{\lambda g} = 4 \text{Re}[\langle \psi_{\lambda+\delta\lambda, g} | \psi_{\lambda, g+\delta g} \rangle - \langle \psi_{\lambda+\delta\lambda, g} | \psi_{\lambda, g} \rangle \langle \psi_{\lambda, g+\delta g} | \psi_{\lambda, g} \rangle] / (\delta\lambda\delta g)$ [67, 68]. The equally-weighted uncertainty in measuring λ and g is given by $\delta\lambda^2 + \delta g^2 \geq G^{-1}$, where

$$G = \frac{\mathcal{F}_{\lambda\lambda} + \mathcal{F}_{gg}}{\mathcal{F}_{\lambda\lambda}\mathcal{F}_{gg} - \mathcal{F}_{\lambda g}\mathcal{F}_{g\lambda}}. \quad (7)$$

As shown in fig. 4(a), G takes a significant value both

in the HO-DTC and the non-DTC phases, but it is not significant in the period-doubling DTC phase. In order to characterize the scaling behavior of G , we have taken a scaling form for $G(t = nT, N_{\text{sat}}) \propto n^\alpha N_{\text{sat}}^\beta$. For classical probes, the best possible sensitivity corresponds to $\beta = 1$; this is known as the standard quantum limit (SQL). By employing quantum resources, it is possible to surpass the SQL and reach the Heisenberg limit (HL) corresponding to $\alpha = \beta = 2$ [69]. As shown in fig. 4(b), HO-DTCs can surpass the SQL with $\alpha = 2$ and $\beta = 1$, when N_{sat} is even. Furthermore, when N_{sat} is odd, it can achieve HL sensitivity with $\alpha = \beta = 2$. The non-DTC regions exhibit significant oscillations of the QFI, thereby making it difficult to obtain a scaling behavior [62]. Thus, our results reveal that DTCs can serve as a powerful resource for multi-parameter sensing, thereby taking a significant step beyond the single-parameter DTC-sensing protocols studied in some recent works [70–73].

Conclusion and Outlook: In this work, we have proposed many-body echo protocols to realize eternal time crystal phases in the driven central spin model. Such eternal time crystals are extremely rare, since TTSB usually can not persist up to infinitely long times in finite-size systems [74]. Floquet systems always synchronize with the drive at long times. Firstly, we have demonstrated that by tuning the interaction strength λ to $2j\pi$ (where $j \in \mathbb{Z}$) it is possible to realize both an eternal period-doubling time crystal and dynamical many-body freezing. Furthermore, eternal HO-DTCs can be realized by tuning λ to $(2j+1)\pi$ and g to $(j'+1/2)\pi$ (where $j' \in \mathbb{Z}$). The dynamics of these HO-DTCs involve non-trivial oscillations of the entanglement entropy, associated with the creation and destruction of Bell-cat states. Thus, our protocol provides a natural route for the rapid preparation of Bell-cat states. Finally, we have demonstrated that these HO-DTCs can be employed for multi-parameter quantum metrology. We conclude that the driven central spin model can serve as a powerful platform to realize a rich array of non-equilibrium phenomena.

There are several natural extensions of this work. Firstly, it would be interesting to investigate the non-equilibrium phases that would emerge in driven central spin- S models with $S > 1/2$. It would also be intriguing to examine the fate of DTC order when interactions are introduced between the satellite spins. Finally, the dynamics of central spin systems subjected to aperiodic driving would be a fruitful avenue for future research.

SC thanks DST, India for support through SERB project SRG/2023/002730.

-
- * sayanchoudhury@hri.res.in
- [1] M. Bukov, L. D'Alessio, and A. Polkovnikov, *Advances in Physics* **64**, 139 (2015).
 - [2] F. Harper, R. Roy, M. S. Rudner, and S. Sondhi, *Annual Review of Condensed Matter Physics* **11**, 345 (2020).
 - [3] M. S. Rudner and N. H. Lindner, *Nature Reviews Physics* **2**, 229 (2020).
 - [4] T. Oka and S. Kitamura, *Annual Review of Condensed Matter Physics* **10**, 387 (2019).
 - [5] C. Weitenberg and J. Simonet, *Nature Physics* **17**, 1342 (2021).
 - [6] T. Banerjee and K. Sengupta, arXiv preprint arXiv:2407.20764 (2024).
 - [7] V. Khemani, A. Lazarides, R. Moessner, and S. L. Sondhi, *Physical Review Letters* **116**, 250401 (2016).
 - [8] C. W. von Keyserlingk, V. Khemani, and S. L. Sondhi, *Physical Review B* **94**, 085112 (2016).
 - [9] N. Y. Yao, A. C. Potter, I.-D. Potirniche, and A. Vishwanath, *Physical Review Letters* **118**, 030401 (2017).
 - [10] D. V. Else, B. Bauer, and C. Nayak, *Physical Review Letters* **117**, 090402 (2016).
 - [11] K. Sacha, *Physical Review A* **91**, 033617 (2015).
 - [12] D. V. Else, C. Monroe, C. Nayak, and N. Y. Yao, *Annual Review of Condensed Matter Physics* **11**, 467 (2020).
 - [13] M. P. Zaletel, M. Lukin, C. Monroe, C. Nayak, F. Wilczek, and N. Y. Yao, *Reviews of Modern Physics* **95**, 031001 (2023).
 - [14] K. Sacha and J. Zakrzewski, *Reports on Progress in Physics* **81**, 016401 (2017).
 - [15] M. Estarellas, T. Osada, V. Bastidas, B. Renoust, K. Sanaka, W. Munro, and K. Nemoto, *Science Advances* **6**, eaay8892 (2020).
 - [16] L. J. I. Moon, P. M. Schindler, R. J. Smith, E. Druga, Z.-R. Zhang, M. Bukov, and A. Ajoy, arXiv preprint arXiv:2410.05625 (2024).
 - [17] J. Zhang *et al.*, *Nature* **543**, 217 (2017).
 - [18] A. Kyprianidis *et al.*, *Science* **372**, 1192 (2021).
 - [19] S. Choi *et al.*, *Nature* **543**, 221 (2017).
 - [20] J. Randall, C. Bradley, F. van der Gronden, A. Galicia, M. Abobeih, M. Markham, D. Twitchen, F. Machado, N. Yao, and T. Taminiau, *Science* **374**, 1474 (2021).
 - [21] W. Beatrez, C. Fleckenstein, A. Pillai, E. de Leon Sanchez, A. Akkiraju, J. Diaz Alcalá, S. Conti, P. Reshetikhin, E. Druga, M. Bukov, and A. Ajoy, *Nature Physics* **19**, 407 (2023).
 - [22] D. Bluvstein *et al.*, *Science* **371**, 1355 (2021).
 - [23] B. Liu *et al.*, *Nature Communications* **15**, 9730 (2024).
 - [24] X. Mi *et al.*, *Nature* **601**, 531 (2022).
 - [25] Z. Bao, S. Xu, Z. Song, K. Wang, L. Xiang, Z. Zhu, J. Chen, F. Jin, X. Zhu, Y. Gao, *et al.*, *Nature Communications* **15**, 1 (2024).
 - [26] H. Xu, J. Zhang, J. Han, Z. Li, G. Xue, W. Liu, Y. Jin, and H. Yu, arXiv preprint arXiv:2108.00942 (2021).
 - [27] V. Khemani, R. Moessner, and S. Sondhi, arXiv preprint arXiv:1910.10745 (2019).
 - [28] K. Sacha, *Time crystals*, Vol. 114 (Springer, 2020).
 - [29] L. D'Alessio and M. Rigol, *Physical Review X* **4**, 041048 (2014).
 - [30] A. Lazarides, A. Das, and R. Moessner, *Physical Review E* **90**, 012110 (2014).
 - [31] S. Choudhury and E. J. Mueller, *Physical Review A* **90**, 013621 (2014).
 - [32] L. Zhang, H. Kim, and D. A. Huse, *Physical Review E* **91**, 062128 (2015).
 - [33] R. Moessner and S. L. Sondhi, *Nature Physics* **13**, 424 (2017).
 - [34] J. Rovny, R. L. Blum, and S. E. Barrett, *Physical Review Letters* **120**, 180603 (2018).
 - [35] J. Rovny, R. L. Blum, and S. E. Barrett, *Physical Review B* **97**, 184301 (2018).
 - [36] S. Pal, N. Nishad, T. Mahesh, and G. Sreejith, *Physical Review Letters* **120**, 180602 (2018).
 - [37] B. Huang, Y.-H. Wu, and W. V. Liu, *Physical Review Letters* **120**, 110603 (2018).
 - [38] A. Pizzi, J. Knolle, and A. Nunnenkamp, *Physical Review Letters* **123**, 150601 (2019).
 - [39] A. Pizzi, J. Knolle, and A. Nunnenkamp, *Nature Communications* **12**, 2341 (2021).
 - [40] M. H. Muñoz-Arias, K. Chinni, and P. M. Poggi, *Physical Review Research* **4**, 023018 (2022).
 - [41] A. Russomanno, F. Iemini, M. Dalmonte, and R. Fazio, *Physical Review B* **95**, 214307 (2017).
 - [42] F. M. Surace, A. Russomanno, M. Dalmonte, A. Silva, R. Fazio, and F. Iemini, *Physical Review B* **99**, 104303 (2019).
 - [43] N. Maskara, A. A. Michailidis, W. W. Ho, D. Bluvstein, S. Choi, M. D. Lukin, and M. Serbyn, *Physical Review Letters* **127**, 090602 (2021).
 - [44] S. Sarkar and Y. Dubi, *ACS Nano* **18**, 27988 (2024).
 - [45] S. Liu, S.-X. Zhang, C.-Y. Hsieh, S. Zhang, and H. Yao, *Physical Review Letters* **130**, 120403 (2023).
 - [46] R. Frantzeskakis, J. Van Dyke, L. Zaporski, D. A. Gangloff, C. Le Gall, M. Atatüre, S. E. Economou, and E. Barnes, *Physical Review B* **108**, 075302 (2023).
 - [47] A. Kumar, R. Frantzeskakis, and E. Barnes, arXiv preprint arXiv:2402.18001 (2024).
 - [48] A. Cabot, F. Carollo, and I. Lesanovsky, *Physical Review B* **106**, 134311 (2022).
 - [49] J. Geng, V. Vorobyov, D. Dasari, and J. Wrachtrup, arXiv preprint arXiv:2107.11748 (2021).
 - [50] B. Vlastakis *et al.*, *Nature Communications* **6**, 8970 (2015).
 - [51] B. Urbaszek, X. Marie, T. Amand, O. Krebs, P. Voisin, P. Maletinsky, A. Högele, and A. Imamoglu, *Reviews of Modern Physics* **85**, 79 (2013).
 - [52] Y. Ashida, T. Shi, R. Schmidt, H. Sadeghpour, J. I. Cirac, and E. Demler, *Physical Review Letters* **123**, 183001 (2019).
 - [53] J. Dobrzyniecki and M. Tomza, *Physical Review A* **108**, 052618 (2023).
 - [54] I. Schwartz *et al.*, *Science Advances* **4**, eaat8978 (2018).
 - [55] L. Childress, M. Gurudev Dutt, J. Taylor, A. Zibrov, F. Jelezko, J. Wrachtrup, P. Hemmer, and M. Lukin, *Science* **314**, 281 (2006).
 - [56] M. Niknam, L. F. Santos, and D. G. Cory, *Physical Review Letters* **127**, 080401 (2021).
 - [57] A. Das, *Physical Review B* **82**, 172402 (2010).
 - [58] S. Bhattacharyya, A. Das, and S. Dasgupta, *Physical Review B* **86**, 054410 (2012).
 - [59] A. Haldar, D. Sen, R. Moessner, and A. Das, *Physical Review X* **11**, 021008 (2021).
 - [60] T. Banerjee, S. Choudhury, and K. Sengupta, arXiv preprint arXiv:2404.06536 (2024).
 - [61] N. Gangopadhyay and S. Choudhury, arXiv preprint arXiv:2409.17198 (2024).

- [62] See supplemental material for details.
- [63] G. Giachetti, A. Solfanelli, L. Correale, and N. Defenu, *Phys. Rev. B* **108**, L140102 (2023).
- [64] B. Lajci, D. O'Dell, and J. Mumford, arXiv preprint arXiv:2410.23532 (2024).
- [65] S. Dooley, F. McCrossan, D. Harland, M. J. Everitt, and T. P. Spiller, *Physical Review A* **87**, 052323 (2013).
- [66] J. Huang, M. Zhuang, B. Lu, Y. Ke, and C. Lee, *Physical Review A* **98**, 012129 (2018).
- [67] J. Liu, H. Yuan, X.-M. Lu, and X. Wang, *Journal of Physics A: Mathematical and Theoretical* **53**, 023001 (2020).
- [68] R. Demkowicz-Dobrzański, W. Górecki, and M. Guță, *Journal of Physics A: Mathematical and Theoretical* **53**, 363001 (2020).
- [69] V. Montenegro, C. Mukhopadhyay, R. Yousefjani, S. Sarkar, U. Mishra, M. G. Paris, and A. Bayat, arXiv preprint arXiv:2408.15323 (2024).
- [70] C. Lyu, S. Choudhury, C. Lv, Y. Yan, and Q. Zhou, *Physical Review Research* **2**, 033070 (2020).
- [71] R. Yousefjani, K. Sacha, and A. Bayat, arXiv preprint arXiv:2405.00328 (2024).
- [72] F. Iemini, R. Fazio, and A. Sanpera, *Physical Review A* **109**, L050203 (2024).
- [73] R. K. Shukla, L. Chotorlishvili, S. K. Mishra, and F. Iemini, *Phys. Rev. B* **111**, 024315 (2025).
- [74] Y. Huang, *New Journal of Physics* **26**, 072001 (2024).

Supplemental Material for ‘The Floquet central spin model: A platform to realize eternal time crystals, entanglement steering, and multiparameter metrology’

In this supplemental material, we provide an alternative analysis of the many-body echo protocol at $\lambda = 2\pi$ and a detailed discussion of the mechanism to realize an eternal higher-order DTC. We have also provided some additional numerical results on the multiparameter sensing protocol.

AN ALTERNATIVE ANALYSIS OF THE MANY-BODY ECHO PROTOCOL AT $\lambda = 2\pi$

In the main text, we have demonstrated that the satellite spin magnetization exhibit perfect period-doubling oscillations when $\lambda = 2\pi$ for all values of g_s . In this section, we provide an alternative derivation of this phenomenon. In particular, we analyze the dynamics of a fully x-polarized initial state, $|\psi(t=0)\rangle = \left(\prod_{i=1}^{N_{\text{sat}}} |+\mathbf{x}\rangle_i\right) |+\mathbf{x}\rangle_c$. In the following analysis, all the states are defined modulo an overall phase. After the first drive period, the system evolves to the state:

$$\begin{aligned} |\psi(t=T)\rangle &= U_0 \left[\left(\prod_{j=1}^{N_{\text{sat}}} (\cos(g_s/2)|+\mathbf{x}\rangle_j - i \sin(g_s/2)|-\mathbf{x}\rangle_j) \right) (\cos(g_c/2)|+\mathbf{x}\rangle_c - i \sin(g_c/2)|-\mathbf{x}\rangle_c) \right] \\ &= \left[\left(\prod_{j=1}^{N_{\text{sat}}} (\cos(g_s/2)|+\mathbf{x}\rangle_j + i \sin(g_s/2)|-\mathbf{x}\rangle_j) \right) (\cos(g_c/2)|+\mathbf{x}\rangle_c - i(-1)^{N_{\text{sat}}} \sin(g_c/2)|-\mathbf{x}\rangle_c/2) \right] \end{aligned} \quad (\text{S1})$$

Consequently, when N_{sat} is odd, we obtain

$$\begin{aligned} |\psi(t=2T)\rangle &= U_0 U_d \left[\left(\prod_{j=1}^{N_{\text{sat}}} (\cos(g_s/2)|+\mathbf{x}\rangle_j + i \sin(g_s/2)|-\mathbf{x}\rangle_j) \right) (\cos(g_c/2)|+\mathbf{x}\rangle_c + i \sin(g_c/2)|-\mathbf{x}\rangle_c/2) \right] \\ &= U_0 \left[\left(\prod_{i=1}^{N_{\text{sat}}} |+\mathbf{x}\rangle_i \right) |+\mathbf{x}\rangle_c \right] = |\psi(t=0)\rangle. \end{aligned} \quad (\text{S2})$$

Thus, both the satellite spin and central spin magnetization show perfect period-doubling oscillations. This situation changes when N_{sat} is even:

$$\begin{aligned} |\psi(t=2T)\rangle &= U_0 U_d \left[\left(\prod_{j=1}^{N_{\text{sat}}} (\cos(g_s/2)|+\mathbf{x}\rangle_j + i \sin(g_s/2)|-\mathbf{x}\rangle_j) \right) (\cos(g_c/2)|+\mathbf{x}\rangle_c - i \sin(g_c/2)|-\mathbf{x}\rangle_c/2) \right] \\ &= U_0 \left[\left(\prod_{i=1}^{N_{\text{sat}}} |+\mathbf{x}\rangle_i \right) (\cos(g_c)|+\mathbf{x}\rangle_c - i \sin(g_c)|-\mathbf{x}\rangle_c) \right] = \left(\prod_{i=1}^{N_{\text{sat}}} |+\mathbf{x}\rangle_i \right) (\cos(g_c)|+\mathbf{x}\rangle_c - i \sin(g_c)|-\mathbf{x}\rangle_c) \end{aligned} \quad (\text{S3})$$

Thus, in this case, the satellite spins exhibit perfect period-doubling oscillations, while the central spin magnetization oscillates sinusoidally.

DETAILED ANALYSIS OF THE MECHANISM TO REALIZE A HIGHER-ORDER TIME CRYSTAL

In this section, we analyze the states generated during the evolution of the eternal HO-DTC, when $\lambda = \pi$ and $g = \pi/2$. We start by noting that in this case for a single spin, $U_d = \exp\left\{-i\frac{\pi}{2}S_z\right\} = \frac{1}{\sqrt{2}} \begin{pmatrix} 1-i & 0 \\ 0 & 1+i \end{pmatrix}$. The following analysis becomes easier to track if one notes that the application of U_d on a single spin takes $|\pm \mathbf{x}\rangle$ to $|\pm \mathbf{y}\rangle$, $|\pm \mathbf{y}\rangle$ to $|\mp \mathbf{x}\rangle$ and $|\pm \mathbf{z}\rangle$ to $|\pm \mathbf{z}\rangle$.

We will first analyze the evolution of one satellite spin for one drive period and then extrapolate the results for N_{sat} spins. Just like the analysis in the previous section, all the states are going to be defined modulo an overall phase. In this case for the x-polarized initial state $|\psi(t=0)\rangle = |+\mathbf{x}\rangle_s |+\mathbf{x}\rangle_c$. Thus after the first drive period, the system evolves to the state :

$$|\psi(t=T)\rangle = U_0 U_d |+\mathbf{x}\rangle_s |+\mathbf{x}\rangle_c = U_0 \left[\frac{1}{2} (|+\mathbf{x}\rangle_s - i|-\mathbf{x}\rangle_s) (|+\mathbf{x}\rangle_c - i|-\mathbf{x}\rangle_c) \right] = \frac{1}{\sqrt{2}} (|+\mathbf{z}\rangle_s |+\mathbf{x}\rangle_c - |-\mathbf{z}\rangle_s |-\mathbf{x}\rangle_c) \quad (\text{S4})$$

It is straightforward to the case of N_{sat} satellite spins, when $|\psi(t=0)\rangle = \left(\prod_{i=1}^{N_{\text{sat}}} |+\mathbf{x}\rangle_i \right) |+\mathbf{x}\rangle_c$. In this case, we obtain

$$|\psi(t=T)\rangle = \frac{1}{\sqrt{2}} \left[\left(\prod_{j=1}^{N_{\text{sat}}} |+\mathbf{z}\rangle_j \right) |+\mathbf{x}\rangle_c + (-1)^{N_{\text{sat}}} \left(\prod_{j=1}^{N_{\text{sat}}} |-\mathbf{z}\rangle_j \right) |-\mathbf{x}\rangle_c \right] \quad (\text{S5})$$

The action of U_d on this state is straightforward, leading to the following state at $t = 3T/2$:

$$|\psi(t=3T/2)\rangle = \frac{1}{\sqrt{2}} \left[\left(\prod_{j=1}^{N_{\text{sat}}} |+\mathbf{z}\rangle_j \right) |+\mathbf{y}\rangle_c + (-i)^{N_{\text{sat}}} \left(\prod_{j=1}^{N_{\text{sat}}} |-\mathbf{z}\rangle_j \right) |-\mathbf{y}\rangle_c \right] \quad (\text{S6})$$

The evolution of the system from $t = 3T/2$ to $t = 2T$ can be split into 4 classes depending on the value of N_{sat}

$$\begin{aligned} N_{\text{sat}} = 4n + 1 &: \frac{1}{\sqrt{2}} \left[\left(\prod_{j=1}^{N_{\text{sat}}} |+\mathbf{y}\rangle_j \right) |+\mathbf{z}\rangle_c + i \left(\prod_{j=1}^{N_{\text{sat}}} |-\mathbf{y}\rangle_j \right) |-\mathbf{z}\rangle_c \right], \\ N_{\text{sat}} = 4n + 2 &: \frac{1}{\sqrt{2}} \left[\left(\prod_{j=1}^{N_{\text{sat}}} |+\mathbf{y}\rangle_j \right) |+\mathbf{y}\rangle_c + i \left(\prod_{j=1}^{N_{\text{sat}}} |-\mathbf{y}\rangle_j \right) |-\mathbf{y}\rangle_c \right], \\ N_{\text{sat}} = 4n + 3 &: \frac{1}{\sqrt{2}} \left[\left(\prod_{j=1}^{N_{\text{sat}}} |+\mathbf{y}\rangle_j \right) |-\mathbf{z}\rangle_c + i \left(\prod_{j=1}^{N_{\text{sat}}} |-\mathbf{y}\rangle_j \right) |+\mathbf{z}\rangle_c \right], \\ N_{\text{sat}} = 4n &: \frac{1}{\sqrt{2}} \left[\left(\prod_{j=1}^{N_{\text{sat}}} |+\mathbf{y}\rangle_j \right) |-\mathbf{y}\rangle_c - i \left(\prod_{j=1}^{N_{\text{sat}}} |-\mathbf{y}\rangle_j \right) |+\mathbf{y}\rangle_c \right], \end{aligned} \quad (\text{S7})$$

where n is a positive integer. Over the course of the drive period, the evolution of the system is quite different for odd and even values of N_{sat} . For even N_{sat} , the system evolves to the following Bell-cat states:

$$\begin{aligned} N_{\text{sat}} = 4n &: \frac{1}{\sqrt{2}} \left[\left(\prod_{j=1}^{N_{\text{sat}}} |+\mathbf{x}\rangle_j \right) |+\mathbf{x}\rangle_c + i \left(\prod_{j=1}^{N_{\text{sat}}} |-\mathbf{x}\rangle_j \right) |-\mathbf{x}\rangle_c \right] \\ N_{\text{sat}} = 4n + 2 &: \frac{1}{\sqrt{2}} \left[\left(\prod_{j=1}^{N_{\text{sat}}} |+\mathbf{x}\rangle_j \right) |-\mathbf{x}\rangle_c + i \left(\prod_{j=1}^{N_{\text{sat}}} |-\mathbf{x}\rangle_j \right) |+\mathbf{x}\rangle_c \right] \end{aligned} \quad (\text{S8})$$

This means that the application of U^3 drives a ‘+x’-polarized state to a Bell-cat state. A further evolution under U^3 will create a ‘+x’-polarized state, and the system will return it to its initial state after 12 periods.

The situation is distinctly different for the odd N_{sat} case as seen in eq (S8). In this case at $t = 3T$, the system

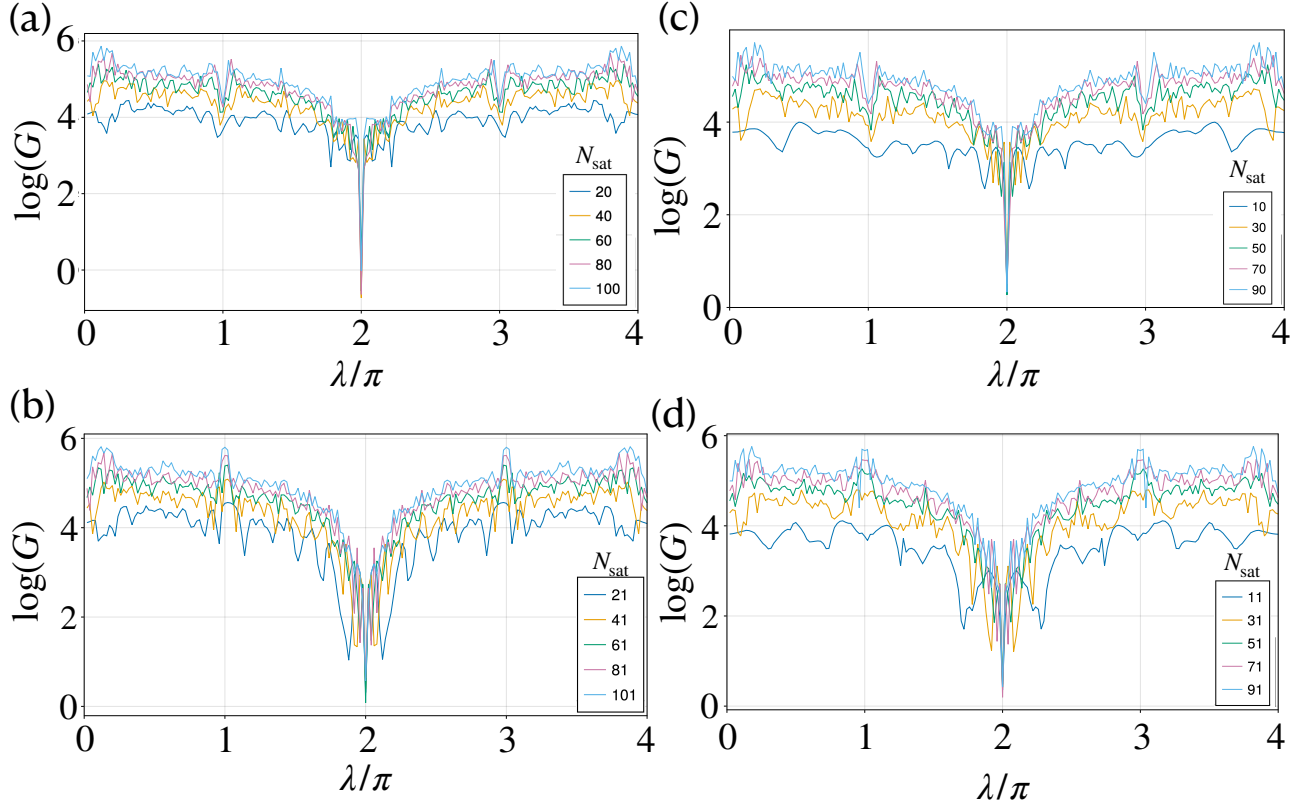


FIG. S1. Dependence of the QFI value, $G(t = 100T)$ (Eq. 7 of the main text) on λ for $N_{\text{sat}} = 4j$ (a), $4j + 1$ (b), $4j + 2$ (c), and $4j + 3$ (d), when $g = \pi/2$. While the non-DTC and HO-DTC regions are both associated with a high value of G , the non-DTC regions exhibit oscillatory behavior that makes it difficult to obtain a system-size dependence; the HO-DTC, on the other hand, exhibits a clear system-size dependence as mentioned in the main text.

evolves to the satellite-spin cat state:

$$N_{\text{sat}} = 4n + 1 : \frac{1}{\sqrt{2}} \left[\left(\prod_{j=1}^{N_{\text{sat}}} |+\mathbf{x}\rangle_j \right) - i \left(\prod_{j=1}^{N_{\text{sat}}} |-\mathbf{x}\rangle_j \right) \right] |+\mathbf{y}\rangle_c \quad (\text{S9})$$

$$N_{\text{sat}} = 4n + 3 : \frac{1}{\sqrt{2}} \left[\left(\prod_{j=1}^{N_{\text{sat}}} |+\mathbf{x}\rangle_j \right) + i \left(\prod_{j=1}^{N_{\text{sat}}} |-\mathbf{x}\rangle_j \right) \right] |+\mathbf{y}\rangle_c$$

The application of the U_d on this state leads to the following state at $t = 3.5T$:

$$N_{\text{sat}} = 4n + 1 : \frac{1}{\sqrt{2}} \left[\left(\prod_{j=1}^{N_{\text{sat}}} |+\mathbf{y}\rangle_j \right) - i \left(\prod_{j=1}^{N_{\text{sat}}} |-\mathbf{y}\rangle_j \right) \right] |-\mathbf{x}\rangle_c \quad (\text{S10})$$

$$N_{\text{sat}} = 4n + 3 : \frac{1}{\sqrt{2}} \left[\left(\prod_{j=1}^{N_{\text{sat}}} |+\mathbf{y}\rangle_j \right) + i \left(\prod_{j=1}^{N_{\text{sat}}} |-\mathbf{y}\rangle_j \right) \right] |-\mathbf{x}\rangle_c$$

Finally at $t = 4T$, both for $N_{\text{sat}} = 4n + 1$ and $N_{\text{sat}} = 4n + 3$, the system evolves to the state,

$$|\psi(t = 4T)\rangle = \frac{1}{\sqrt{2}} \left[\left(\prod_{j=1}^{N_{\text{sat}}} |+\mathbf{z}\rangle_j \right) - \left(\prod_{j=1}^{N_{\text{sat}}} |-\mathbf{z}\rangle_j \right) \right] |-\mathbf{x}\rangle_c, \quad (\text{S11})$$

as mentioned in eq. 5 in the main text. Thus, the central spin magnetization oscillates with a period of $12T$, when N_{sat} is odd. However, the satellite spin magnetization oscillates with a period of $24T$. To see this, we note that at

$t = 6T$, the system evolves to the Bell-cat state:

$$|\psi(t = 6T)\rangle = \frac{1}{\sqrt{2}} \left(\prod_{j=1}^{N_{\text{sat}}} |+\mathbf{x}\rangle_j \right) |+\mathbf{x}\rangle_c - i \left(\prod_{j=1}^{N_{\text{sat}}} |-\mathbf{x}\rangle_j \right) |-\mathbf{x}\rangle_c \quad (\text{S12})$$

Analogous to our analysis for the even N_{sat} case, we can conclude that the magnetization would oscillate with a period of $24T$. These results are corroborated in the magnetization and entanglement entropy evolution plots given in fig. 3 of the main text.

Before concluding this section, we recall that in our discussion on multi-parameter metrology in the main text, we had found that both the HO-DTC and non-DTC parameter regimes were associated with a high value of the G (defined in eq. 7 of the main text). Furthermore, we had demonstrated that HO-DTCs exhibit a QFI scaling of $G(t = nT, N_{\text{sat}}) \propto n^\alpha N_{\text{sat}}^\beta$, where $\alpha = 2$ for any value of N_{sat} and $\beta = 2$ and 1 for odd and even values of N_{sat} . As shown in fig. S1 however, such a systematic dependence can not be obtained for non-DTC regions due to the oscillatory nature of G in this parameter regime.
